Cell- and stimulus-dependent heterogeneity of synaptic vesicle endocytic recycling mechanisms revealed by studies of dynamin 1-null neurons

Mitsuko Hayashi*†, Andrea Raimondi*, Eileen O'Toole‡, Summer Paradise*, Chiara Collesi§, Ottavio Cremona§, Shawn M. Ferguson*, and Pietro De Camilli*¶‖

*Department of Cell Biology, Program in Cellular Neuroscience, Neurodegeneration and Repair, Howard Hughes Medical Institute and ¶Department of Neurobiology, Kavli Institute for Neuroscience, Yale University School of Medicine, New Haven, CT 06510; ‡Boulder Laboratory for 3D Electron Microscopy of Cells, Department of Molecular, Cellular and Developmental Biology, University of Colorado, Boulder, CO 80309; and §FIRC Institute of Molecular Oncology Foundation (IFOM), and Università Vita-Salute San Raffaele, 20139 Milan, Italy

Contributed by Pietro De Camilli, December 22, 2007 (sent for review December 13, 2007)

Mice lacking expression of dynamin 1, a GTPase implicated in the fission reaction of synaptic vesicle endocytosis, fail to thrive and exhibit severe activity-dependent endocytic defects at their synapses. Here, we have used electron tomography to investigate the massive increase in clathrin-coated pit abundance that is selectively observed at a subset of synapses in dynamin 1 KO primary neuron cultures under conditions of spontaneous network activity. This increase, leading to branched tubular plasma membrane invaginations capped by clathrin-coated buds, occurs selectively at inhibitory synapses. A similar massive increase of clathrin-coated profiles (in this case, of clathrin-coated vesicles) is observed at inhibitory synapses of neurons that lack expression of synaptojanin 1, a phosphoinositide phosphatase involved in clathrin-coated vesicle uncoating. Thus, although excitatory synapses are largely spared under these conditions, inhibitory synapses are uniquely sensitive to perturbation of endocytic proteins, probably as a result of their higher levels of tonic activity leading to a buildup of clathrin-coated intermediates in these synapses. In contrast, the predominant endocytic structures observed at the majority of dynamin 1 KO synapses after acute stimulation are endosome-like intermediates that originate by a dynamin 1-independent form of endocytosis. These findings reveal a striking heterogeneity in the mode of synaptic vesicle recycling in different synapses and functional states.

clathrin | electron microscopy | endocytosis | synapse | synaptojanin

Synaptic vesicles (SVs) are continuously regenerated by endocytosis at presynaptic nerve terminals (1–8). Strong evidence has implicated the GTPase dynamin in this recycling process, more specifically in the fission of deeply invaginated clathrin-coated buds from the plasma membrane (9–13). Disruption of dynamin function in a variety of organisms and cell types has a strongly negative effect on several pathways of endocytosis (9, 13–19). In addition, cell free studies have demonstrated the ability of dynamin to sever narrow membrane tubules, at least under certain experimental conditions (20, 21).

Mammals express three dynamin isoforms. Dynamin 1, by far the most abundant dynamin at synapses, is surprisingly not essential for synaptic transmission and early postnatal life (15). However, nerve terminals of neurons lacking dynamin 1 exhibit functional and structural defects that are consistent with an impairment of synaptic vesicle recycling. These include delayed internalization of synaptic vesicle membrane proteins and an increased accumulation of endocytic clathrin-coated pits (CCPs) (15). More specifically, in primary neuronal cultures from dynamin 1 KO mice, spontaneous network activity induced an accumulation of CCPs that was on average greater than in wild-type (WT) neurons and was massive at a subset of synapses. This effect increased with cell plating density and with the age of the cultures, two conditions that favor increased neuronal connectivity and activity. Conversely, this accumulation was reversed by silencing electrical activity with the Na^+ channel blocker tetrodotoxin (TTX) (15).

The action of dynamin in nerve endings is thought to be tightly linked to the action of synaptojanin 1, a polyphosphoinositide phosphatase that dephosphorylates phosphatidylinositol 4,5-bisphosphate [$PI(4,5)P_2$] on endocytic membranes. $PI(4,5)P_2$ functions at the plasma membrane as a major membrane coreceptor for endocytic factors, including the clathrin adaptors and dynamin itself. Thus, synaptojanin 1 is thought to couple fission of endocytic vesicles to the dephosphorylation of $PI(4,5)P_2$ needed for the shedding of such factors (22, 23). Nerve terminals of synaptojanin 1 KO mice, which die shortly after birth, exhibit an accumulation of clathrin-coated profiles that is reminiscent of the one observed at dynamin 1 KO synapses and is massive at a small subset of synapses, although clathrin-coated vesicles (CCVs), rather than CCPs, accumulate in these terminals (22).

We have now further analyzed structural changes produced by the absence of dynamin 1 and synaptojanin 1 at synapses. Our results provide insight into the heterogeneity of synaptic vesicle membrane recycling mechanisms in different neuronal populations and in different functional states.

Results and Discussion

Massive Accumulation of Clathrin-Coated Pits in a Dynamin 1 KO Nerve Terminal. We have reported a partial electron tomographic reconstruction of a dynamin 1 KO nerve terminal containing a massive number of clathrin-coated structures (15). A complete 3D reconstruction of membranous organelles in an 800-nm-thick volume of the same nerve terminal further demonstrates the profound impairment of clathrin-mediated endocytosis at the stage of deeply invaginated pits (Fig. 1). As shown by an analysis of the 3D model (Fig. 1*A*; see also supporting information (SI) Movies 1–6) and by the single tomographic slice shown in Fig. 1*B* (slice 245 of a total of 432 slices), the bulk of the nerve terminal is occupied by clathrin-coated profiles (green in Fig. 1 *A* and *N*), whereas two synaptic vesicle clusters (blue spheres) occupy only a very small portion of the nerve terminal next to

Author contributions: M.H., A.R., S.M.F., and P.D.C. designed research; M.H., A.R., S.P., and S.M.F. performed research; M.H., A.R., E.O., C.C., O.C., S.M.F., and P.D.C. contributed new reagents/analytic tools; M.H., A.R., S.P., S.M.F., and P.D.C. analyzed data; and M.H., S.M.F., and P.D.C. wrote the paper.

The authors declare no conflict of interest.

Freely available online through the PNAS open access option.

†Present address: Faculty of Bioscience, Nagahama Institute of Bio-Science and Technology, Nagahama, Shiga 526-0829, Japan.

‖To whom correspondence should be addressed. E-mail: pietro.decamilli@yale.edu.

This article contains supporting information online at www.pnas.org/cgi/content/full/0712171105/DC1.

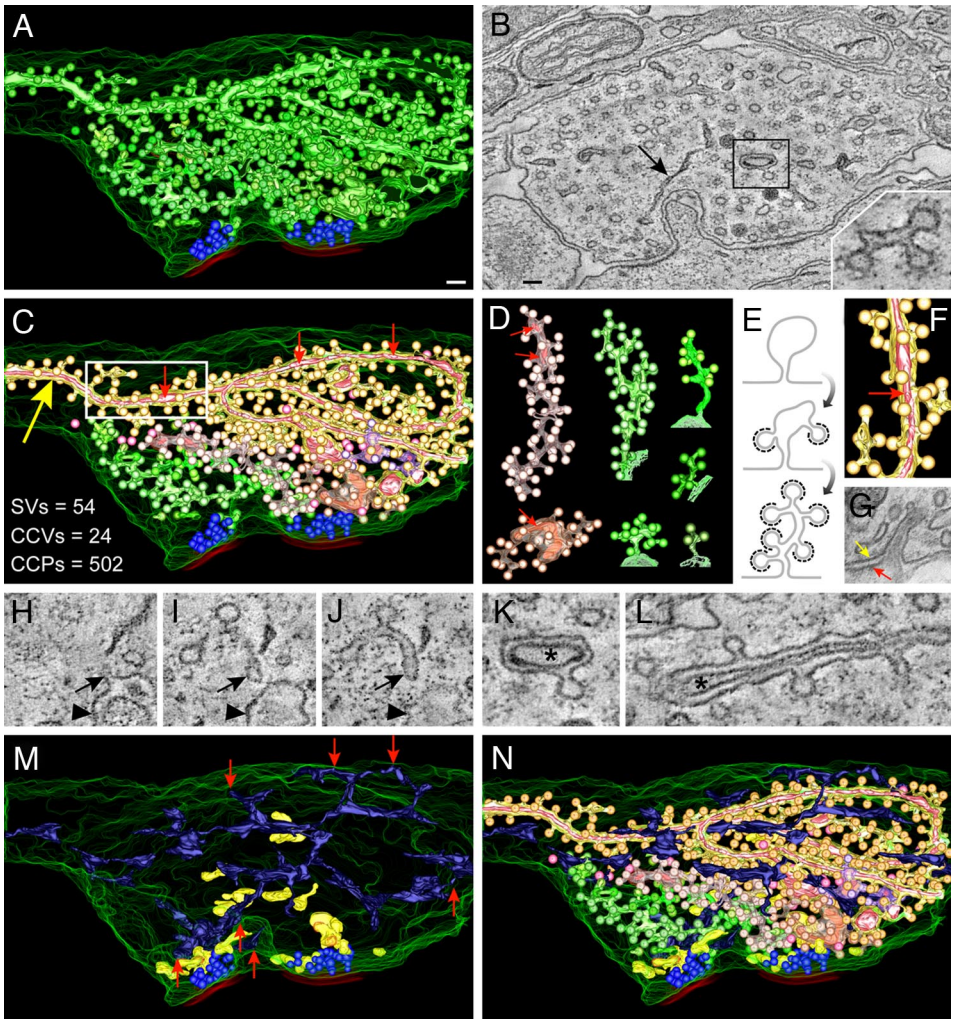

Fig. 1. Tomogram and 3D models of a dynamin 1 KO synapse containing an extreme abundance of CCPs. (*A*) 3D model of the synapse showing SVs and all clathrin-coated structures. SVs are blue spheres, the plasma membrane is outlined by a series of green curves, and red lines indicate selected postsynaptic membranes. The overwhelming majority of coated structures shown in green originate from tubular membranes. (*B*) Tomographic slice (slice 245 of 432) of the reconstructed volume. Most vesicular profiles are clathrin-coated and appear as buds when viewed in the appropriate tomographic plane (see *Inset*). A black arrow points to the ER. (*C*) The independent CCP decorated tubules are depicted in different colors. The numbers summarize the abundance of the indicated structures in this reconstruction. CCVs are shown as pink spheres. (*D*) Examples of individual reconstructed tubules from the image shown in *C*. For the green tubules, the site of origin at the plasma membrane is shown. (*E*) Hypothetical model of how tubules could be generated through the assembly and arrest of clathrin-coated buds on plasma membrane infoldings. (*F*) Magnification of the boxed region in *C* demonstrating the presence of another membrane (bright pink) within the large tubule (orange-yellow). (*G*) Electron micrograph of a structure that may represent the cell surface origin of a tubule such as the one shown in *F*. Yellow and red arrows represent the plasma membranes of the two adjacent cells. (*H–J*) Tomographic slices (13-nm intervals) revealing the continuity with the plasma membrane (arrowhead) of a tubular structure (open arrows) decorated with CCPs. (*K* and *L*) Tomographic slices of the tubule shown in *F* revealing the internal membrane (asterisks; see also boxed region in *B*). (*M*) 3D modeling of other membranous organelles present in the tomogram: endosome-like structures (yellow) and smooth ER (dark blue). Red arrows point to regions of contact between the ER and the plasma membrane (see also SI Fig. 6). (*N*) A 3D model of the reconstructed nerve terminal volume including all membranous organelles shown (see also SI Fig. 6). (Scale bars, 100 nm.)

active zones and thus opposite to postsynaptic membranes (red). Only very few, scattered, CCVs were observed (Fig. 1*C* and SI Fig. 6 *A–C*, pink spheres).

Within this synapse, CCPs (several hundreds) were ≈10-fold more abundant than SVs, whereas in control synapses CCPs represent on average <2% of SVs (numbers of SVs, CCPs, and CCVs are given in the Fig. 1*C Inset*; see also Fig. 2 *D–F* for comparison). Most of the CCPs were connected to each other by narrow tubular structures [each shown in different shades of green and pink (Fig. 1 *C* and *D*, see also SI Movie 2)], with occasional dilations, which in most cases can be seen to originate directly from the plasma membrane within the volume of the tomogram. The diagram of Fig. 1*E* depicts a potential mechanism through which assembly and then arrest of clathrin-coated buds on plasma membrane infoldings may underlie their formation. The many dynamin-binding proteins that have the capability to generate and/or stabilize narrow membrane tubules by BAR and F-BAR domains (24) are candidates to play a role in the formation (or abnormal growth) of these tubular structures in the absence of dynamin 1 function.

Surprisingly, some of the tubules contained another membrane within their lumen (bright pink, indicated by small red arrows in Fig. 1 *C* and *F*). A striking example is the large tubule indicated by a large yellow arrow in Fig. 1*C* and in two tomographic slices in Fig. 1 *K* and *L* (see also SI Movie 3). The outer surface of this tubule accounts for 58% of the CCPs visible in the entire tomogram. Although the origin of this particular tubule is outside of the reconstructed region, such a structure may

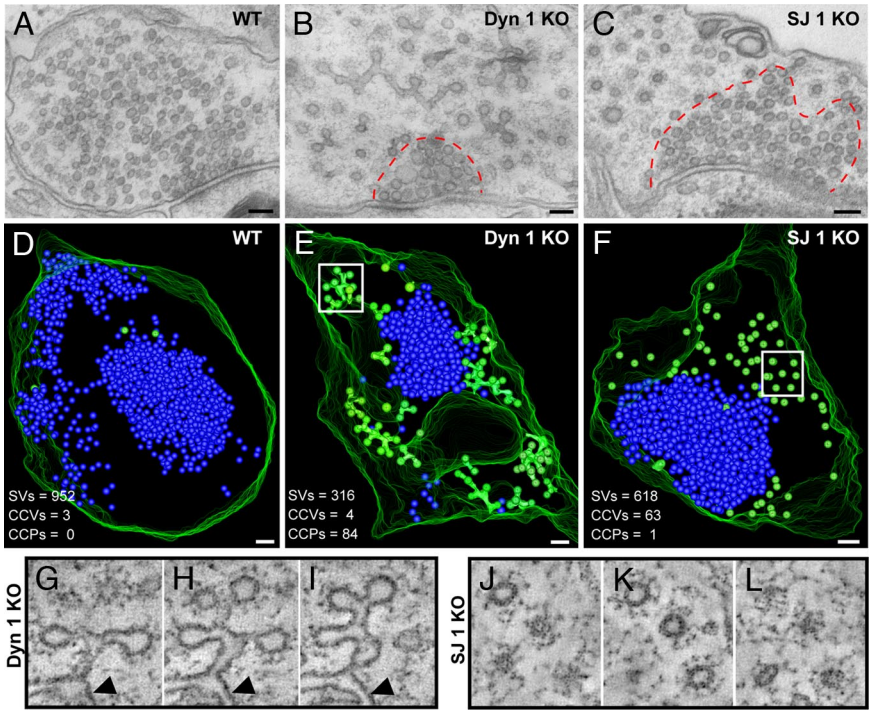

Fig. 2. Ultrastructure of synapses enriched in clathrin-coated intermediates from wild-type, dynamin 1 KO, and synaptojanin 1 KO neurons. (*A–C*) Conventional electron micrographs. Note the abundance of clathrin-coated profiles in *B* and *C* and the less dense packing of these structures relative to the packing of SVs (enclosed by dashed red lines). (*D–F*) 3D models from 250-nm-thick tomograms showing that the bulk of coated profiles (green) are buds in dynamin 1 KO synapses and free vesicles in synaptojanin 1 KO synapses. SVs are shown in blue. (*G–I*) Tomographic slices (8-nm intervals) of the boxed region in *E* (an arrowhead indicates the plasma membrane). (*J–L*) Tomographic slices (17-nm intervals) of the boxed region in *F*. (Scale bars, 100 nm.)

represent a great exaggeration of spinules present at normal synapses: small clathrin-coated invaginations of the plasma membrane containing an evagination from an adjacent cell (25). Indeed such structures were observed in single sections of both WT and dynamin 1 KO cultures (Fig. 1*G*).

Other membranous organelles present in the tomogram were also modeled. The endoplasmic reticulum (ER) (dark blue, Fig. 1 *M* and *N*; SI Movie 4) formed a continuous network of tubulo-cisternal structures that were interspersed with, but clearly distinct from, the CCP-decorated tubules (see also three tomographic slices in SI Fig. 6 *E–G*). Heterogeneously sized vacuoles, more abundant in proximity to the synaptic vesicle clusters and clearly disconnected from the ER, the coated pit network, and the plasma membrane likely represent endosomes or endosome-like structures (6, 26) (yellow, Fig. 1 *M* and *N* and SI Fig. 6*D*). A model of all reconstructed membrane structures within the entire 800-nm-thick tomogram is shown in Fig. 1*N*, SI Fig. 6, and SI Movie 5 (see also SI Table 1 for additional details).

Comparison of Dynamin 1 KO and Synaptojanin 1 KO Nerve Terminals. Although frequently observed in low-power EM observation of dynamin 1 KO neuronal cultures, synapses where the bulk of SVs was replaced by CCPs (such as the synapse shown in Fig. 1) represented a minority of the entire synaptic population (see also ref. 15). A striking accumulation of clathrin-coated structures at only a small subset of synapses was observed in cultures of synaptojanin 1 KO neurons (22, 27). In view of this similarity, a direct comparison was performed between the effects produced by the two genotypes relative to WT in neuronal cultures grown under similar conditions. In both KO genotypes, electron microscopy revealed a variable abundance of clathrin-coated profiles, ranging from none in sections of some terminals to a massive accumulation in sections of other terminals (Fig. 2 *A–C*). Three-dimensional reconstructions from electron tomograms of 250-nm-thick sections (Fig. 2 *D–F*) showed that the overwhelming majority of coated profiles (green spheres) were buds in dynamin 1 KO neurons and free vesicles in synaptojanin 1 KO neurons. Electron tomography also revealed the extremely low abundance of clathrin-coated profiles in WT neurons (Fig. 2*D*).

Similar increases in the extent of clathrin-coated profile (CCPs or CCVs) accumulation in dynamin 1 and synaptojanin 1 KO nerve terminals was further supported by immunofluorescence analysis. Immunoreactivity for components of clathrin coats, namely clathrin light chain, α-adaptin (AP-2 subunit), and AP180 (28, 29), was much more intense and punctate relative to WT controls in both KO genotypes (Fig. 3), a finding known to correlate with a high number of assembled coats (15). Dynamin 3, previously shown to undergo a striking clustering in dynamin 1 KO cultures (15), was surprisingly (because one would expect release of dynamin after fission) similarly clustered in synaptojanin 1 KO cultures (Fig. 3). The clustering of dynamin 3 in synaptojanin 1 KO neurons may arise from interactions with actin regulatory proteins (30) or the clathrin coat whose assembly is stimulated by the increase in $PI(4,5)P_2$ resulting from defective synaptojanin 1 function (31). No obvious differences between WT and the two mutant genotypes were observed in the distribution of immunoreactivity for bassoon (32), a marker of active zones of secretion used as a control (Fig. 3). These changes in the appearance of immunoreactivity for endocytic proteins must be explained by their redistribution because their total levels in the cultures as established by SDS/PAGE and Western blotting were unchanged relative to control (15, 22).

Clustering of Coat Proteins in Dynamin 1 KO and Synaptojanin 1 KO Neurons Occurs Predominantly at Inhibitory Synapses. In both dynamin 1 KO and synaptojanin 1 KO neuron cultures the largest accumulation of clathrin-coated pits occurs in a subset of neurons under conditions that favor spontaneous network ac-

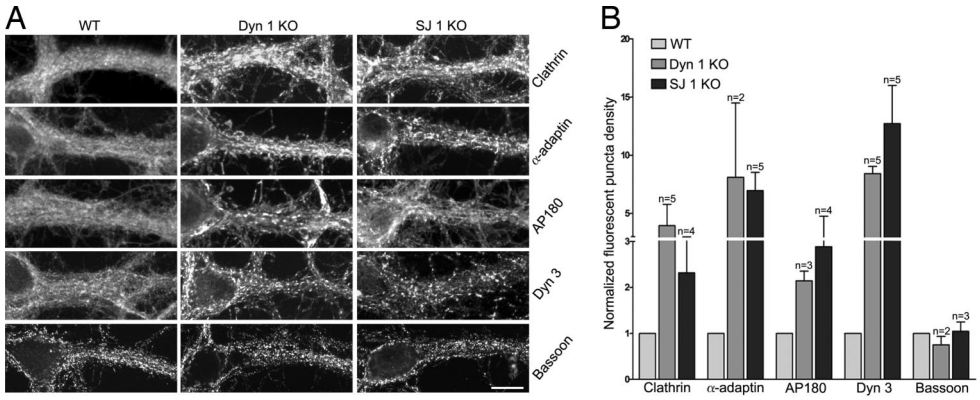

Fig. 3. Enhanced clustering of endocytic proteins in the absence of either dynamin 1 or synaptojanin 1. (*A*) Cortical neurons in culture were fixed and stained by immunofluorescence for the proteins indicated. (Scale bar, 15 μm.) (*B*) Quantification of the endocytic protein-clustering data. Counted puncta (see *Experimental Procedures*) were expressed as the number of puncta per 100 μm^2 and then normalized for the value of control samples. In the two conditions for which $n = 2$, the mean $\pm$ standard deviation is presented. Elsewhere, the bars show the mean $\pm$ SEM of multiple independent experiments (n). The y axis represents the fold of increase of puncta in dynamin 1 KO and synaptojanin KO versus their respective WT control cultures.

tivity, and this accumulation is reversed by silencing electrical activity with TTX (15; data not shown). Thus, we considered the possibility that a similar subset of neurons was uniquely sensitive to endocytic perturbations produced by the absence of either dynamin 1 or synaptojanin 1 because of their high level of tonic activity. Because high levels of activity are observed in inhibitory (GABA-ergic) neuron subpopulations of the cerebral cortex (33), and given that these neurons represent a minority of all neurons in our primary cortical cultures, the subset of dynamin 1 KO and synaptojanin 1 KO neurons with the greatest abundance of presynaptic CCPs and CCVs, respectively, might be GABAergic interneurons. When cultures of both genotypes were analyzed by double immunofluorescence to correlate abundance of clathrin coats with the neurotransmitter phenotype, the brightest and largest puncta positive for clathrin coat components and dynamin 3 colocalized with the vesicular GABA transporter (VGAT, a marker of inhibitory synapses), but not with vesicular glutamate transporters [VGLUT1, a marker of excitatory synapses (Fig. 4; see also SI Fig. 7). We conclude that under conditions of spontaneous network activity the greatest synaptic vesicle recycling defects occur in inhibitory neurons and note that enhanced levels of endocytic proteins have been reported at tonically active synapses in the lamprey nervous system (34). Furthermore, the reversal of the presynaptic clathrin machinery clustering phenotype after treatment of dynamin 1 and synaptojanin 1 KO neurons with TTX emphasizes that these neurons maintain a synaptic vesicle recycling capacity that is adequate to keep pace with low rates of synaptic vesicle exocytosis.

Endosome-Like Structures Observed After Acute Massive Stimulation. We next investigated whether a strong acute stimulus could induce a generalized accumulation of CCPs at all dynamin 1 KO synapses. We had previously shown that a 90-sec high K^+ stimulation of dynamin 1 KO neurons produced a more striking reduction in total SV number than in WT neurons, leading to a nearly complete depletion of these vesicles (15). Surprisingly, we also found that after this stimulation the abundance of nerve terminals with a massive content of clathrin-coated profiles (such as the example shown in Fig. 1) remained relatively low. Instead, in the great majority of other KO synapses, the bulk of SVs had been replaced by large vacuoles (compare Fig. 5 *A* with *B*), whose endocytic nature was demonstrated by their loading with the extracellular tracer horseradish peroxidase (HRP) added during the stimulation (Fig. 5*C*). A similar change was also observed at the majority of WT synapses after stimulation. However, the reduction of SV number and the compensatory accumulation of endocytic vacuoles was less striking in these nerve terminals (sections through WT synapses contained 5.1 $\pm$ 1.0 HRP-labeled endosomes compared with 10.5 $\pm$ 1.7 in KO synapses, t test $P < 0.01$) in these control cultures (Fig. 5*D* and SI Fig. 8). Although the finding that during massive stimulation SV membranes are recaptured primarily by bulk endocytosis is not new (6, 35–38), the striking and unexpected result is that this process occurs in the absence of dynamin 1.

A 3D model derived from the tomographic analysis of a 500-nm-thick volume of endosome-rich KO synapses after the high K^+ stimulation is shown in Fig. 5 *E* and *F* (see also SI Movie 6). Only a few scattered SVs (blue, Fig. 5 *E* and *F*) are present, whereas endosome-like structures (yellow) disconnected from the plasma membrane similar to those shown in Fig. 1*M* are extremely abundant (Fig. 5*E*). Tubules connected to the plasma

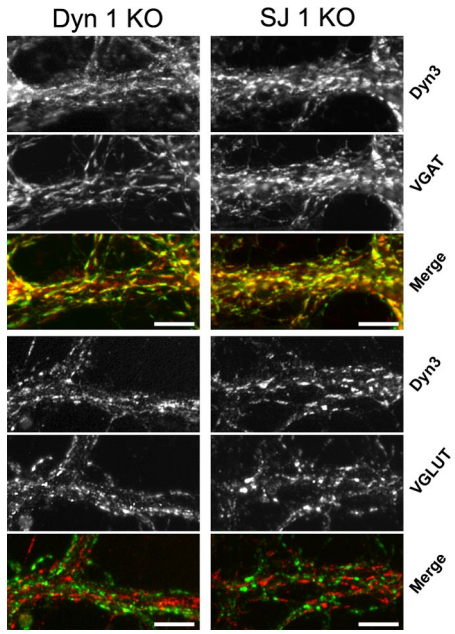

Fig. 4. The enhanced clustering of endocytic proteins in dynamin 1 and synaptojanin 1 KO neurons occurs selectively at inhibitory synapses. Dynamin 1 and synaptojanin 1 KO cortical neurons in culture were fixed and stained by immunofluorescence for the indicated proteins. (Scale bars, 10 μm.)

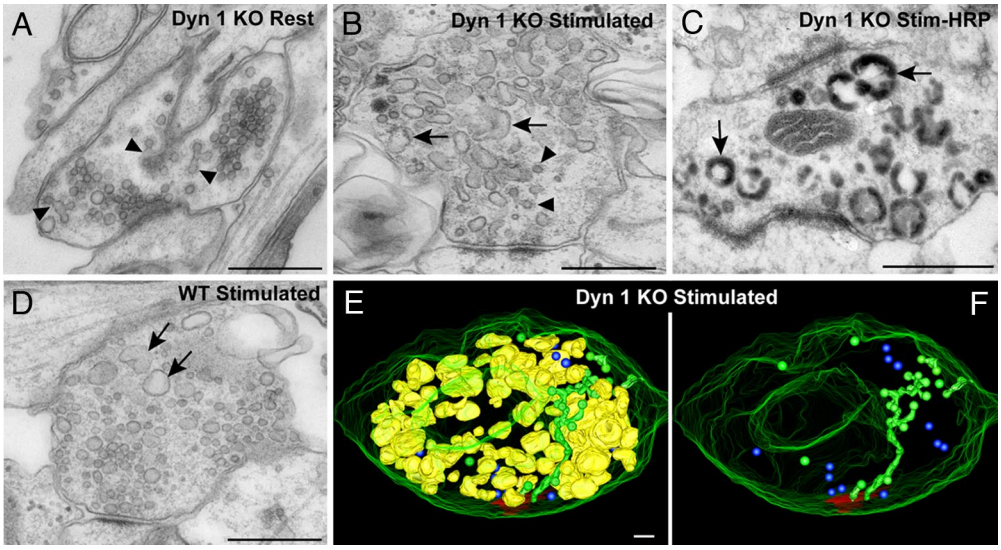

Fig. 5. Effects of high K^+ mediated depolarization on the ultrastructure of dynamin 1 KO synapses. (*A*) Example of a dynamin 1 KO nerve terminal kept in control medium in which SVs by far predominate despite an abnormal accumulation of CCPs (arrows). (*B*) Dynamin 1 KO nerve terminal fixed at the end of a 90-sec-long high K^+ (90 mM KCl). Note the near absence of SVs, the presence of some CCPs (arrowheads), and the great abundance of vacuoles/endosomes. (*C*) Dynamin 1 KO synapse incubated with HRP during the high K^+ stimulus. (*D*) Stimulated WT synapse. Vacuoles are present, but SVs are still very abundant. (*E*) 3D model of a 500-nm-thick volume of a stimulated KO synapse demonstrating SVs (blue spheres), selected postsynaptic membranes (red), endosomes (yellow), and clathrin-coated endocytic intermediates (green). (*F*) Same image as *E*, after the subtraction of the endosomes. (Scale bars, *A–D*, 500 nm; *E* and *F*, 100 nm.)

membrane and decorated by CCPs (green) are also visible (Fig. 5 *E* and *F*), but they clearly account for only a small fraction of internal membranes. Such strong stimulatory conditions may not favor, or may not be permissive for, efficient clathrin coat assembly, for example, because of a stimulation-dependent drop in the level of $PI(4,5)P_2$ (39), a critical factor in endocytic clathrin coat nucleation (29, 40, 41).

A 10-min recovery from the 90-sec high K^+ stimulus resulted in the re-formation of SVs and the disappearance of endosome-like intermediates both in WT and in dynamin 1 KO cultures (albeit less efficiently in KO cultures) (15). The mechanisms underlying the conversion of endosome-like intermediates into new SVs remains an important open question. The lack of CCP accumulation on these structures both in WT, but especially in dynamin 1 KO synapses, suggests that a mechanism distinct from direct clathrin-mediated budding is involved.

The efficient formation of endosome-like structures in dynamin 1 KO synapses during a high K^+ stimulation is surprising given that synaptopHluorin-based assays of synaptic vesicle recycling in these mutant neurons detected a profound endocytic defect during field stimulation (300 action potentials at 10 Hz) (15). This discrepancy may reflect the different type and intensity of stimulation, because differences in endocytic pathways in response to different modes of stimulation have been reported (36, 42). However, further studies are needed to clarify the relationship between stimulation protocols and the engagement of distinct endocytic mechanisms.

Concluding Remarks. Our findings provide new insight into structural changes produced by the absence of dynamin 1. They demonstrate a more critical dependence of inhibitory than of excitatory synapses on the clathrin-dependent synaptic vesicle recycling machinery for the maintenance of a normal pool of synaptic vesicles. They also bring into new focus long-standing questions concerning the importance of clathrin-mediated endocytosis and bulk endocytosis in SV recycling (1, 6, 37). The spectacular accumulation of clathrin-coated profiles observed at a subset of dynamin 1 and synaptojanin 1 KO nerve terminals (predominantly or exclusively inhibitory synapses) demonstrates the presence of a very large reservoir of clathrin coat components and further establishes the importance of clathrin-mediated endocytosis as a physiological mechanism of SV retrieval and re-formation that predominates under tonic activity. However, the occurrence of a dynamin 1-independent form of bulk endocytosis, which predominates in response to a prolonged depolarization stimulus and is followed by a dynamin 1-independent generation of new SVs, open new questions on recycling pathways leading to SVs that may be independent of clathrin-mediated endocytosis.

Experimental Procedures

All procedures involving mice were approved by the Yale University Institutional Animal Care and Use Committee. Primary cultures of cortical neurons were prepared from P0–P2 brains by previously described methods, plated at a density of 15,000–50,000 cells per cm^2, and analyzed at 16–26 days *in vitro* (15, 43). These conditions were selected because they yielded large numbers of clathrin-coated intermediates in dynamin 1 KO neurons. Neurons were maintained in Neurobasal medium, 2% B27 supplement, 0.5 mM L-glutamine, penicillin/streptomycin (all media components from Invitrogen). For experiments involving stimulation, the neurons were preincubated for 90 sec at 37°C in 119 mM NaCl, 2.5 mM KCl, 2 mM $CaCl_2$, 2 mM $MgCl_2$, 25 mM Hepes, and 30 mM glucose, and then stimulated for 90 sec in 90 mM KCl buffer ([NaCl] reduced accordingly to maintain osmolarity) and fixed at the end of the stimulus. In some experiments HRP (10 mg/ml, Sigma) was included in the buffer and neurons were briefly rinsed (several seconds in ice-cold buffer) before fixation. HRP-positive endosomes (outer diameter, >80 nm) were counted from a total of 27 WT and 20 KO synapses from two independent WT and KO littermate cultures.

Immunofluorescence was performed on neurons fixed in 4% paraformaldehyde, 4% sucrose, 0.1 M sodium phosphate, pH 7.4, as described (15). The following commercial antibodies were used: mouse anti α-adaptin (Affinity Bioreagents), mouse anti-Bassoon (Stressgen Biotechnologies), rabbit anti-VGAT, mouse anti-VGLUT1 (Synaptic Systems), guinea pig anti-VGLUT1 and mouse anti-VGLUT2 (Chemicon). Antibodies generated in the De Camilli laboratory and described include: mouse anti-AP180, mouse anti-dynamin 3, and rabbit anti-dynamin 3 (15). Rabbit anti-clathrin light chain was a kind gift from Peter McPherson (McGill University, Montreal, Canada). Alexa488 and Alexa594 conjugated secondary antibodies were purchased from Invitrogen. The samples were examined with a Zeiss Axioplan2 microscope with a Plan-Apochromatic 40× objective. Images of randomly selected KO and control neurons were acquired with a Hamamatsu ORCA II digital camera under the

same gain and exposure parameters. The images were processed with MetaMorph v7.1.2 (Molecular Devices) using the application *Count Nuclei* able to detect bright fluorescent puncta over a diffuse background. For each experiment ($n = 1$), between 10 and 20 regions of interest were analyzed from a single culture from the respective WT and KO genotypes.

For electron microscopy cells were fixed with 1.3% glutaraldehyde in 66 mM sodium cacodylate buffer, postfixed in 1% OsO_4, 1.5% $K_4Fe(CN)_6$, 0.1M sodium cacodylate, stained with 0.5% uranyl magnesium acetate, dehydrated, and embedded in Embed 812. Where indicated, HRP reactions were developed with diaminobenzidene and H_2O_2 after the glutaraldehyde fixation step. Electron microscopy reagents were purchased from Electron Microscopy Sciences. Ultrathin sections were observed in a Philips CM10 microscope at 80 kV and images were taken with a Morada 2k $\times$ 2k CCD camera (Olympus).

For electron tomography, 200-nm-thick and 250-nm-thick sections were examined in either a TECNAI F20 or a F30 intermediate-voltage microscope operating at 200 kV or 300 kV (Boulder Laboratory for 3-D Electron Microscopy of Cells, University of Colorado). Tilt series data for each section were recorded around two orthogonal axes (1° intervals over a $\pm$ 60° for each axis) by using the Serial-EM image acquisition program (44) and a Gatan 2k $\times$ 2k CCD camera at a pixel size of 1 nm. Tomograms from up to four serial sections were computed and joined by using the IMOD software package (44, 45). The resolution of all reconstructed tomograms in 3D was 4–6 nm. Subcellular structures within the 3D volume were segmented and their surfaces were modeled. For the generation of the final models, contours of membranes were traced manually, but small vesicular structures SVs, CCVs, and CCPs were displayed as spheres.

ACKNOWLEDGMENTS. We thank Frank Wilson, Lijuan Liu, Louise Lucast, and Livia Tomasini for superb technical assistance, as well as P. McPherson for antibodies. This work was supported in part by the G. Harold and Leila Y. Mathers Charitable Foundation; National Institutes of Health Grants NS36251, CA46128, DK45735, and DA018343 (to P.D.C.); National Institutes of Health National Center for Research Resources Grant RR-000592 (to J. R. McIntosh, University of Colorado, Boulder, CO); Association Italiana per la Ricerca sul Cancro (AIRC), Association for International Cancer Research (AICR-UK), Telethon Grant GGP05141, INTERLINK project of the Italian Ministry of University and Research, Programmi di Ricerca Scientifica di Rilevante Interesse Nazionale (PRIN2006) (to O.C.); a Canadian Institutes of Health Research fellowship (to S.M.F.); and a Human Frontiers Science Program fellowship (to M.H.).

1. Jung N, Haucke V (2007) Clathrin-mediated endocytosis at synapses. *Traffic* 8(9):1129–1136.
2. Ryan TA (2006) A pre-synaptic to-do list for coupling exocytosis to endocytosis. *Curr Opin Cell Biol* 18:416–421.
3. Granseth B, Odermatt B, Royle SJ, Lagnado L (2006) Clathrin-mediated endocytosis is the dominant mechanism of vesicle retrieval at hippocampal synapses. *Neuron* 51:773–786.
4. Murthy VN, De Camilli P (2003) Cell biology of the presynaptic terminal. *Annu Rev Neurosci* 26:701–728.
5. Brodin L, Low P, Shupliakov O (2000) Sequential steps in clathrin-mediated synaptic vesicle endocytosis. *Curr Opin Neurobiol* 10:312–320.
6. Heuser JE, Reese TS (1973) Evidence for recycling of synaptic vesicle membrane during transmitter release at the frog neuromuscular junction. *J Cell Biol* 57:315–344.
7. Ceccarelli B, Hurlbut WP, Mauro A (1973) Turnover of transmitter and synaptic vesicles at the frog neuromuscular junction. *J Cell Biol* 57:499–524.
8. Augustine GJ, *et al.* (2006) Clathrin and synaptic vesicle endocytosis: Studies at the squid giant synapse. *Biochem Soc Trans* 34:68–72.
9. Damke H, Baba T, Warnock DE, Schmid SL (1994) Induction of mutant dynamin specifically blocks endocytic coated vesicle formation. *J Cell Biol* 127:915–934.
10. Hinshaw JE (2000) Dynamin and its role in membrane fission. *Annu Rev Cell Dev Biol* 16:483–519.
11. Praefcke GJ, McMahon HT (2004) The dynamin superfamily: Universal membrane tubulation and fission molecules? *Nat Rev Mol Cell Biol* 5:133–147.
12. Takei K, McPherson PS, Schmid SL, De Camilli P (1995) Tubular membrane invaginations coated by dynamin rings are induced by GTP-gamma S in nerve terminals. *Nature* 374:186–190.
13. Koenig JH, Ikeda K (1989) Disappearance and reformation of synaptic vesicle membrane upon transmitter release observed under reversible blockage of membrane retrieval. *J Neurosci* 9:3844–3860.
14. Macia E, *et al.* (2006) Dynasore, a cell-permeable inhibitor of dynamin. *Dev Cell* 10:839–850.
15. Ferguson SM, *et al.* (2007) A selective activity-dependent requirement for dynamin 1 in synaptic vesicle endocytosis. *Science* 316:570–574.
16. Herskovits JS, Burgess CC, Obar RA, Vallee RB (1993) Effects of mutant rat dynamin on endocytosis. *J Cell Biol* 122:565–578.
17. Clark SG, *et al.* (1997) A dynamin GTPase mutation causes a rapid and reversible temperature-inducible locomotion defect in *C. elegans*. *Proc Natl Acad Sci USA* 94:10438–10443.
18. Henley JR, Krueger EW, Oswald BJ, McNiven MA (1998) Dynamin-mediated internalization of caveolae. *J Cell Biol* 141:85–99.
19. Shupliakov O, *et al.* (1997) Synaptic vesicle endocytosis impaired by disruption of dynamin-SH3 domain interactions. *Science* 276:259–263.
20. Roux A, Uyhazi K, Frost A, De Camilli P (2006) GTP-dependent twisting of dynamin implicates constriction and tension in membrane fission. *Nature* 441:528–531.
21. Sweitzer SM, Hinshaw JE (1998) Dynamin undergoes a GTP-dependent conformational change causing vesiculation. *Cell* 93:1021–1029.
22. Cremona O, *et al.* (1999) Essential role of phosphoinositide metabolism in synaptic vesicle recycling. *Cell* 99:179–188.
23. McPherson PS, Takei K, Schmid SL, De Camilli P (1994) p145, a major Grb2-binding protein in brain, is co-localized with dynamin in nerve terminals where it undergoes activity-dependent dephosphorylation. *J Biol Chem* 269:30132–30139.
24. Itoh T, De Camilli P (2006) BAR, F-BAR (EFC) and ENTH/ANTH domains in the regulation of membrane-cytosol interfaces and membrane curvature. *Biochim Biophys Acta* 1761:897–912.
25. Spacek J, Harris KM (2004) Trans-endocytosis via spinules in adult rat hippocampus. *J Neurosci* 24:4233–4241.
26. Takei K, Mundigl O, Daniell L, De Camilli P (1996) The synaptic vesicle cycle: A single vesicle budding step involving clathrin and dynamin. *J Cell Biol* 133:1237–1250.
27. Kim WT, *et al.* (2002) Delayed reentry of recycling vesicles into the fusion-competent synaptic vesicle pool in synaptojanin 1 knockout mice. *Proc Natl Acad Sci USA* 99:17143–17148.
28. De Camilli P, Takei K (1996) Molecular mechanisms in synaptic vesicle endocytosis and recycling. *Neuron* 16:481–486.
29. Owen DJ, Collins BM, Evans PR (2004) Adaptors for clathrin coats: Structure and function. *Annu Rev Cell Dev Biol* 20:153–191.
30. Gray NW, Kruchten AE, Chen J, McNiven MA (2005) A dynamin-3 spliced variant modulates the actin/cortactin-dependent morphogenesis of dendritic spines. *J Cell Sci* 118:1279–1290.
31. Gad H, *et al.* (2000) Fission and uncoating of synaptic clathrin-coated vesicles are perturbed by disruption of interactions with the SH3 domain of endophilin. *Neuron* 27:301–312.
32. tom Dieck S, *et al.* (1998) Bassoon, a novel zinc-finger CAG/glutamine-repeat protein selectively localized at the active zone of presynaptic nerve terminals. *J Cell Biol* 142:499–509.
33. Swadlow HA (2003) Fast-spike interneurons and feedforward inhibition in awake sensory neocortex. *Cereb Cortex* 13:25–32.
34. Evergren E, Zotova E, Brodin L, Shupliakov O (2006) Differential efficiency of the endocytic machinery in tonic and phasic synapses. *Neuroscience* 141(1):123–131.
35. Coggins MR, Grabner CP, Almers W, Zenisek D (2007) Stimulated exocytosis of endosomes in goldfish retinal bipolar neurons. *J Physiol* 584:853–865.
36. de Lange RP, de Roos AD, Borst JG (2003) Two modes of vesicle recycling in the rat calyx of Held. *J Neurosci* 23:10164–10173.
37. Teng H, Lin MY, Wilkinson RS (2007) Macroendocytosis and endosome processing in snake motor boutons. *J Physiol* 582:243–262.
38. Holt M, Cooke A, Wu MM, Lagnado L (2003) Bulk membrane retrieval in the synaptic terminal of retinal bipolar cells. *J Neurosci* 23:1329–1339.
39. Audigier SM, Wang JK, Greengard P (1988) Membrane depolarization and carbamoylcholine stimulate phosphatidylinositol turnover in intact nerve terminals. *Proc Natl Acad Sci USA* 85:2859–2863.
40. Zoncu R, *et al.* (2007) Loss of endocytic clathrin-coated pits upon acute depletion of phosphatidylinositol 4,5-bisphosphate. *Proc Natl Acad Sci USA* 104:3793–3798.
41. Di Paolo G, De Camilli P (2006) Phosphoinositides in cell regulation and membrane dynamics. *Nature* 443:651–657.
42. Wu LG, Ryan TA, Lagnado L (2007) Modes of vesicle retrieval at ribbon synapses, calyx-type synapses, and small central synapses. *J Neurosci* 27:11793–11802.
43. Luthi A, *et al.* (2001) Synaptojanin 1 contributes to maintaining the stability of GABAergic transmission in primary cultures of cortical neurons. *J Neurosci* 21:9101–9111.
44. Mastronarde DN (2005) Automated electron microscope tomography using robust prediction of specimen movements. *J Struct Biol* 152:36–51.
45. Kremer JR, Mastronarde DN, McIntosh JR (1996) Computer visualization of three-dimensional image data using IMOD. *J Struct Biol* 116:71–76.